Pilot-Scale NO_x and SO_x Aftertreatment by Semi-Dry Plasma-Chemical Hybrid Process in Glass-Melting-Furnace Exhaust Gas*

Haruhiko Yamasaki[1], Yuta Mizuguchi[1], Ryosuke Nishioka[1], Yuta Fukuda[1], Tomoyuki Kuroki[1], Hashira Yamamoto[2], and Masaaki Okubo[1]

[1]Department of Mechanical Engineering, Osaka Prefecture University, 1-1 Gakuen-cho, Naka-ku, Sakai 599-8531, Japan

[2]Environmental Affairs Office, Nihon Yamamura Glass Co., Ltd. 15-1 Nishimukojima-cho, Amagasaki-Shi, Hyogo 660-8580, Japan

Abstract The plasma-chemical hybrid process (PCHP) has been effectively employed for the simultaneous removal of NO_x and SO_x in combustion gases. In this study, a PCHP-based semi-dry-type desulfurization reactor was developed for high-temperature exhaust gas from a glass melting furnace with a 10-MW-class thermal input. The NO in the exhaust gas is oxidized to NO_2 by ozone generated from scale-up dielectric barrier discharge-based plasma ozonizers with a total input power of 77 kW and total ozone generation of 10 kg/h. SO_2 reacts with NaOH solution in the semi-dry reactor to produce Na_2SO_3, which further reacts with NO_2 to reduce NO_x to N_2. The produced Na_2SO_4 is in the form of dry particles and can be collected and reused in glass manufacturing. The exhaust gas at the outlet of the semi-dry reactor is maintained between 200 and 250°C to protect the dry-type electrostatic precipitator. A localized cooling area is created by spraying cooling water, which is necessary to prevent the thermal decomposition of ozone and to spray an efficient aqueous solution for achieving dry conditions at the reactor outlet. Simultaneous desulfurization and denitrification were tested at low glass-production rates by injecting adequate flow rates of ozone for NO removal. Optimal removal efficiencies of 45 and 39% were obtained for NO and NO_x, respectively. More than 90% of the byproducts were recovered in the form of Na_2SO_4. The designed facility with the semi-dry-type PCHP was confirmed to be highly effective and promising for exhaust gas treatment in glass manufacturing.

Keywords: Scale-up plasma, Denitration, Desulfurization, Glass manufacturing, Nonthermal plasma, Nitrogen oxides (NO_x), Ozone, Plasma process, Sulfur oxides (SO_x).

Haruhiko Yamasaki (email corresponding author)
Department of Mechanical Engineering, Graduate School of Engineering, Osaka Prefecture University, 1-1 Gakuen-cho, Naka-ku, Sakai 599-8531, Japan.
E-mail: hyamasaki@me.osakafu-u.ac.jp

*The final publication of this paper is
Yamasaki H, Mizuguchi Y, Nishioka R, Fukuda Y, Kuroki T, Yamamoto H, Okubo M., Pilot scale NO_x and SO_x after treatment by semi-dry plasma-chemical hybrid process in glass-melting furnace exhaust gas. Plasma Chem Plasma Process (2021). https://doi.org/10.1007/s11090-021-10193-4
This paper is available at https://link.springer.com/article/10.1007%2Fs11090-021-10193-4

Introduction

Air pollutants such as nitrogen oxides (NO_x) and sulfur oxides (SO_x) cause significant and persistent social and environmental problems. The glass manufacturing industry produces vast quantities of NO_x (which include NO and NO_2) and SO_x. Glass materials are typically melted in furnaces at ~1500°C using fossil fuels, such as heavy oil and city natural gas. The exhaust gas generated in this process contains large amounts of NO_x and SO_x, owing to high-temperature combustion, and raw materials and fuels, respectively. Technologies such as selective catalytic reduction (SCR) [1] followed by wet flue gas desulfurization with chemical agents, such as calcium carbonate and sodium hydroxide [2, 3], are currently employed for NO_x and SO_2 reduction; these are utilized globally for flue gas treatments in coal-fired and oil-fired thermal power plants. However, the catalysts employed in SCR get clogged because the exhaust gases that evolve from the glass melting furnaces contain alkali metals, sulfur, and other compounds that originate from the glass materials [4]. Therefore, current emission regulations on glass melting furnaces focus on the use of low NO_x burners [5] or suppression of NO_x levels during combustion with a low excess-air-ratio. Advanced treatments are required to remove NO_x emissions from exhaust gas. Moreover, a high volume of carbon monoxide emissions is also observed, owing to the high fuel consumption and incomplete combustion. Therefore, the development of an aftertreatment technology that can sufficiently reduce NO_x emissions in exhaust gases from glass melting furnaces is crucial.

Sulfur dioxide (SO_2) readily reacts with alkaline solutions, such as NaOH [6]. Therefore, SO_2 is treated using an NaOH solution in semi-dry or wet desulfurization reactors, which generates particulate matter such as sodium sulfite (Na_2SO_3) and sodium sulfate (Na_2SO_4). These fine particles are typically collected by an electrostatic precipitator or a bag filter that is setup downstream of the reactor. Na_2SO_4, a byproduct of this process, can be reused as a raw material in glass manufacturing [7]. These exhaust gas treatment systems have been extensively employed to minimize the environmental impact of glass melting furnaces; they can also be economical and can help in realizing environmental load reduction.

A highly efficient and energy-conserving atmospheric nonthermal plasma technology, featuring a plasma-chemical hybrid process (PCHP) without catalysts, has been extensively investigated for the removal of NO_x in combustion gases released from boilers, diesel generators, and garbage incinerators [8–17]. PCHP combines the following processes: a plasma process that oxidizes NO in the combustion exhaust gas released from boilers using ozone generated by atmospheric nonthermal plasma and a process involving the reductive removal of NO_2 that is generated via the oxidation of NO with an aqueous Na_2SO_3 solution. PCHPs avoid the problem of catalyst poisoning because of the absence of catalysts in these processes. Furthermore, the hybrid process can be incorporated into the existing wet and semi-dry desulfurization equipment in glass melting furnaces. Therefore, it is possible to realize a low-cost exhaust-gas-treatment system and incur considerably low equipment remodeling costs. In our previous study, a laboratory-scale PCHP [18–21] designed for a 1/50,000 scale of actual exhaust gas volume was investigated, and a pilot-scale experimental exhaust gas treatment was conducted to simulate the exhaust gas conditions of a glass melting furnace. The results of these previous studies demonstrated high levels of denitration and desulfurization using semi-dry PCHP.

Previous studies on such systems have reported a low denitration rate [22, 23], although it was high relative to the quantity of injected ozone; this was because of the insufficient quantity of injected ozone (moles of O_3/moles of NO =< 0.28). In the present study, a pilot-scale experiment was conducted in an actual semi-dry-type aftertreatment system in a glass melting furnace, in combination with two-phase ozone injection using a three-fluid nozzle and a chemical process using a two-fluid nozzle. To achieve a high level of denitration, the quantity of injected ozone (0.31 < moles of O_3/moles of NO < 0.95) was increased using a scale-up plasma ozonizer; the nozzle angle was also increased to improve the chemical reaction time, based on observations from a previous study [23].

Principles of PCHP and the aftertreatment system

The semi-dry PCHP involves a hybrid desulfurization and denitrification technology that combines the plasma process that uses air-reactive gases generated from a nonthermal plasma reactor (mainly O_3), and a chemical process (featuring NaOH as a reducing agent and neutralizer) to remove NO_x and SO_2. In the plasma process, NO in the exhaust gas is oxidized via reaction (1) to water-soluble NO_2 by the O_3 generated from the nonthermal plasma reactor, which uses oxygen gas as a raw material. Because ozone thermally decomposes at temperatures above 150°C, cooling water is simultaneously sprayed with ozone using a two-phase flow nozzle; this forms a localized cooling area with a temperature below 150°C, which facilitates the oxidation of NO by ozone. Some of the ozone self-decomposes into oxygen radicals via reaction (2), and NO is subsequently oxidized by the oxygen radicals via reaction (3).

In glass melting furnaces, SO_2 generated from the fuel and raw materials is readily neutralized by spraying an aqueous NaOH solution, as shown in reaction (4); this reaction generates Na_2SO_3, which has strong reducing properties. This Na_2SO_3 causes the liquid-phase reduction of NO_2 to N_2 gas, and Na_2SO_3 is subsequently oxidized to Na_2SO_4 via reaction (5). Following its semi-dry state, Na_2SO_4 is completely dried by the heat of the exhaust gas. Furthermore, the Na_2SO_4 particles are collected by an electrostatic precipitator and bag filter and are reused in the glass manufacturing system.

$$NO + O_3 \rightarrow NO_2 + O_2 \quad (1)$$

$$O_3 \rightarrow O_2 + O \quad (2)$$

$$NO + O \rightarrow NO_2 \quad (3)$$

$$2NaOH + SO_2 \rightarrow Na_2SO_3 + H_2O \quad (4)$$

$$2NO_2 + 4Na_2SO_3 \rightarrow N_2 + 4Na_2SO_4 \quad (5)$$

Experimental methods

Experimental apparatus

The experiments were conducted using a semi-dry-type exhaust gas aftertreatment system for a glass furnace at the Nihon Yamamura Glass Tokyo Plant (Kanagawa, Japan). **Figure 1** shows an overview of the aftertreatment system, which mainly consists of a semi-dry reactor, electrostatic precipitator (ESP), bag filter, and stack. The exhaust gas from the combustion furnace is initially desulfurized and denitrified in the semi-dry reactor, and the dust produced in the semi-dry reactor is subsequently collected in the electrostatic precipitator. The bag filter subsequently collects the particles that are not removed by the electrostatic precipitator, and the treated gas is discharged from the stack. The furnace can process 245 ton/day of raw glass materials via the combustion of heavy

oil and liquefied natural gas (LNG) at flow rates of 1300 L/h and 100 m^3/h, respectively. The thermal input for the furnace is ~10 MW. The internal temperature of the furnace is maintained at ~1550°C by controlling the flow rates of the fuel and combustion air. A set of combustion burners, located on the north and south sides, is installed inside the furnace. Three burners are located on each side (north and south direction), and their use is alternated every 20 min to facilitate heat exchange with the regenerative furnace. The thermal energy of the exhaust gas is reused in this manner to heat the air required for combustion.

Figure 2 shows a schematic diagram of the semi-dry-type aftertreatment reactor with a plasma-combined chemical process for the glass melting furnace. The reactor features a cylindrical apparatus (ϕ 3.5 × 15 m; Asahi Glass Engineering Co., Ltd.) containing three-fluid-type spray nozzles (seven nozzles, GSIM6055II; H. Ikeuchi & Co., Ltd.) for gas cooling O_3 and two-fluid spray nozzles (seven nozzles, GSIM2037II; H. Ikeuchi & Co., Ltd.) for desulfurization. Water, compressed air, and O_3 are sprayed using the three-fluid nozzles via a pump (CR3-12, 50 Hz, 1.1 kW, 3.0 m^3/h; Grundfos Pumps K.K.). The absorbent solution and compressed air in the two-fluid nozzles are sprayed via another pump (HC, 50 Hz, 3.7 kW, 5 m^3/h; Honda Kiko Co., Ltd.). The three-fluid nozzles are oriented vertically upward at 30° and mounted at z = 1.85 m downstream from the reactor inlet. The two-fluid nozzles are installed horizontally with the tip of the nozzle pointing upward by 30° and are mounted at z = 3.85 m downstream from the reactor inlet. A schematic of the nozzle arrangement in the three-fluid and two-fluid spray nozzles is shown in **Figure 3**. The two-fluid and three-fluid nozzles are installed at the same position in the cross-sectional direction (x–y plane) and 40° apart in the circumferential direction, respectively. Using the three-fluid nozzle, a water mist is formed by spraying compressed air (0.2 MPa) and soft water (0.80 m^3/h, 0.2 MPa) with a sprayed droplet size of 50 μm (Sauter mean diameter). O_3 is released into the localized gas-cooled region formed by the three-fluid-type spray, and a portion of the O_3 is absorbed by the sprayed water. Gaseous O_3 and the O_3 adsorbed by water exist in the localized gas-cooled region as two-phase O_3.

Using the two-fluid nozzle, a solution containing NaOH mist is formed by spraying compressed air (0.2 MPa) and NaOH solution (0.2–0.7 m^3/h, 0.2 MPa) with a sprayed droplet size of 40 μm (Sauter mean diameter). The reaction of SO_2 in the exhaust gas with NaOH produces SO_3^{2-} as a byproduct in the localized cooling area. Additionally, the NO_2 generated via O_3 injection reacts with SO_3^{2-} and transforms into N_2 and a solution containing SO_4^{2-} ions, which dries and transforms into a dust of Na_2SO_4 particles near the outlet of the reactor.

The dried Na_2SO_4 particles present in the exhaust gas are collected downstream of the reactor by a dry-type ESP (negative maximum DC voltage of −45 kV, maximum current of 200 mA, total dust collection area of 879 m^2; Asahi Glass Engineering Co., Ltd.), which is operated at an applied DC voltage between -29 kV and -23 kV; the current is controlled between 61 and 75 mA. The collected dust is subsequently reused as a raw material for glass production. After the ESP, the bag filter (cylindrical filter size = ϕ 155 mm × 6 m, 448 filters, filtration area of 1308 m^2; Asahi Glass Engineering Co., Ltd.) cleanses the dust from the gas to produce a highly cleaned exhaust gas, which is released from the stack into the atmosphere. At the ESP's operating temperature range of 200 to 250°C, the electrical resistivity of collected dust was measured and was in the range of 1.2×10^6 to 1.2×10^8 Ω·cm for various moisture conditions. Therefore, the dust can be

properly collected by the ESP.

Scale-up plasma ozonizer

A total ozone generation rate of ~10 kg/h can be injected into the reactor by combining two scale-up plasma ozonizers (SAGT4M-C and SAGT6M-C; Sumitomo Precision Products Co., Ltd.) in parallel. The detailed specifications of the plasma ozonizers are listed in **Table 1**. The SAGT4M-C plasma ozonizer is depicted in **Figure 4**. Both ozonizers are composed of nonthermal plasma reactors and supplied with O_2 gas from a cold evaporator (CE) tank filled with liquid O_2. After adjusting the pressure of oxygen from the CE tank to 0.13 MPa, flow rates of 26.7 and 40.0 m^3N/h are fed into the SAGT6M-C and SAGT4M-C ozonizers, respectively. The ozone mass flow rate can be adjusted from 0 to 6 kg/h (in SAGT6M-C) and from 0 to 4 kg/h (in SAGT4M-C) by changing the output of the high-voltage power supply unit. The concentration of O_3 generated from the ozonizer is measured using ultraviolet-absorbing ozone monitors (EG-600; 0–200 $g/(m^3N)$; Ebara Jitsugyo Co., Ltd.). The SAGT6M-C and SAGT4M-C ozonizers consist of 432 and 334 glass plasma reactors, respectively, and the glass plasma reactors are cooled with water at 15°C to maintain a constant ozone output even during long-term operation. A detailed schematic of one of the glass plasma reactors in the ozonizer is presented in **Figure 5**, along with a picture of the arrangement of the various parts of SAGT6M-C. The glass plasma reactor consists of a glass electrode and a water-cooled ground electrode and can generate plasma via dielectric barrier discharge between the electrodes. Further, the 1400-mm-long glass plasma reactors are installed while considering the point symmetry.

Experiments

To evaluate the NO_x and SO_x aftertreatment performance of the semi-dry PCHP, the concentrations of the exhaust gas components, such as SO_2, NO, and NO_x, are measured at the inlet and outlet of the reactor, as shown in **Figure 2**, using SO_2 analyzers (IRA-208 Shimadzu Corporation and VA-3000, PG-337, and PG-350, Horiba, Ltd.), NO analyzers (PG-240, PG-337, PG-340, and PG-350; Horiba, Ltd.), and NO_x analyzers (NOA7000, NOA7100, and IRA-208; Shimadzu Corporation). The concentration of each gas (NO, NO_x, SO_2, and O_2) significantly varies with changes in the direction of combustion in the furnace. The concentration data are assumed to follow a t-distribution to reject irregular data; the two-sided probability is calculated, and the data are processed with a significance level of 20%. NO_x and SO_x concentrations are expressed as equivalent values based on an oxygen concentration of 15% using $A = B(21–15)/(21–C)$, where A is the converted NO_x or SO_x concentration based on O_2 = 15%, B is the measured NO_x or SO_x concentration, and C is the measured O_2 concentration.

Furthermore, the temperature of the exhaust gas is measured at the following points to confirm the formation of the localized cooling area: the inlet and outlet of the reactor and four locations inside the reactor (z = 0, 2.85, 4.35, and 5.85 m; four locations downstream). The detailed setup featuring the temperature measurement points inside the reactor is depicted in **Figure 6**. Five points each are measured at heights of z = 2.85 and 4.35 m, respectively, and three points are measured at z = 5.85 m. The flow rate and water content of the exhaust gas at the inlet and outlet of the reactor are measured using a pitot tube-type flow meter and a moisture absorption tube, respectively, in accordance with the

Japanese Industrial Standard (JIS) Z8808. The volumetric flow rate of the exhaust gas (dry base) is calculated using the measured flow velocity, water content of the exhaust gas, cross-sectional area of the pipe, average gas temperature, and static average pressure at the measurement point. The concentration of oxygen at the reactor inlet and outlet are measured using an Orsat gas analyzer, in accordance with JIS K0301.

Results and discussion

Table 2 lists the experiments conducted from Oct. 2019 to Aug. 2020 that investigated variations in parameters such as the flow rates of O_3 gas, water spray, NaOH solution spray, and concentration of NaOH. The parameters are varied between the tests and continuously measured for 60 min when no ozone is injected and for 120 min when ozone is injected. The flow rate of the exhaust gas on a dry basis is varied between 11550 and 14700 m^3N/h. The temperature range of the reactor inlet is between 390 and 442°C. The concentrations of NO, NO_x, and SO_2 range from 190 to 245 ppm, 196 to 248 ppm, and 272 to 436 ppm, respectively. The average O_2 concentrations are 6.9% and 9.2%, respectively. The experimental parameters for the various test groups are summarized henceforth: test group (1) in Oct. 2019—total glass production rate of 112 ton/day, thermal input of 7 MW to the furnace, combustion air ratio (air/fuel equivalence ratio) of 1.09, and relatively low water and solution spray flow rates of O_3 and NaOH, respectively; test group (2) in Nov. 2019—a higher glass production rate of 156 ton/day, thermal input of 8 MW, air ratio of 0.98, and relatively low water and solution spray flow rates of O_3 and NaOH, respectively; test group (3) in July 2020—a higher glass production rate of 184 ton/day during the T1–T3 periods and 141 ton/day during T4–T7, thermal inputs of 9 MW during T1–T3 and 8 MW during T4–T7, higher air ratios of 1.02 during T1–T3 and 1.05 during T4–T7, and higher water and solution spray flow rates for O_3 and NaOH; test group (4) in Aug. 2020—glass production of 177 ton/day, thermal input of 9 MW, higher air ratio of 1.03, higher water and solution spray flow rates for O_3 and NaOH, and higher NaOH concentrations in the range of 3.0−4.0%. Here, the air ratio is obtained by correcting the theoretical air ratio of the fuel and the usage ratio. As noted earlier, all gas concentrations are expressed in terms of the converted values based on an oxygen concentration of 15%. O_3 gas is injected into the gas-cooled area at mass flow rates of 4.9–11.2 kg/h, and the NaOH concentration is varied from 1.5 to 4.0 mass%.

In the following section, the data obtained from July 2020 (i.e., test group 3 in **Table 2**) are analyzed to investigate the performance of the system; these are representative data that feature successful denitrification and desulfurization.

Temperature distribution

Figure 7 shows the temperature transition of the exhaust gas at z = 0 m (reactor inlet), 2.85 m (reactor interior), 4.35 m (reactor interior), and reactor outlet in the T1–T3 test period (July 2020). The temperatures at z = 2.85 and 4.35 m depicted in the figure represent the averages of their five respective temperature points, as shown in **Figure 6**. The combustion characteristics of the north and south regenerative furnaces are different because of their continuous operation for more than 10 years. Consequentially, the temperature also differs between the north and south furnaces. The temperature at the reactor inlet before the exhaust gas treatment is noted to be in the 384–469°C range, with an average of 432°C. The temperature at the reactor outlet, which is cooled by the

spraying of water and NaOH aqueous solution, is in the 207–258°C range, with an average of 237°C. These results reveal that the exhaust gas at the reactor outlet is completely dry. Therefore, the temperature above the SO_3 dew point and the operating temperature of the dust collector are both realized. The gas at a height of z = 2.85 m, which is 1 m higher than the location of the three-fluid spray nozzle, is cooled to an average temperature of 239°C because of the gas being cooled by the water spray flow rate from the three-fluid spray nozzle. In the upper-reactor region, the gas at a height of z = 4.35 m, which is 0.5 m higher than the two-fluid spray nozzle, is cooled even further to an average temperature of 209°C. The calculated reaction time in the localized cooling region between 1.85 and 3.85 m is 2.6 s, which is sufficient for facilitating the denitration and desulfurization reactions.

Nitrogen monoxide oxidation

Figure 8 shows the time-dependent NO concentrations at the reactor inlet and outlet in the T1–T3 period (July 2020). The NO concentrations are converted based on an oxygen concentration of 15%. The average NO concentrations at the reactor inlet and outlet in the T1, T2, and T3 periods are noted to be 225 ± 15, 199 ± 25, and 211 ± 22 ppm, and 223 ± 14, 116 ± 16, and 116 ± 14 ppm, respectively. In the T1 period, NO concentrations at the inlet and outlet of the reactor are nearly the same, which implies that NO oxidation does not occur because of other factors, such as O_2. In the T2 and T3 periods, NO at the reactor outlet is oxidized to NO_2, and the concentration of NO decreases upon the injection of O_3 into the localized cooling area formed by the three-fluid nozzles. The molar ratios of the injected O_3 to NO in the exhaust gas during the T2 and T3 periods are 0.71 and 0.66, respectively, as listed in **Table 2**. The ratio of the difference in molar flow rates of NO at the reactor inlet and outlet to the molar flow rate of the injected O_3 ($\Delta NO/O_3$) during the T2 and T3 periods are obtained as 67 and 76%, with NO removal efficiencies of 42 and 45%, respectively. Ozone thermally decomposes at high temperatures (>150°C), as shown in reaction (2). Some of the O radicals produced by this thermal decomposition facilitate the oxidation of NO via reaction (3), whereas the remaining O radicals react with O_3 to form oxygen, as expressed in reaction (6).

$$O_3 + O \rightarrow 2O_2 \qquad (6)$$

In a previous study featuring laboratory experiments [18], the $\Delta NO/O_3$ ratio was reported as ~10% at a gas temperature of 300°C in the absence of water spraying. When the gas was cooled to 80°C via water spraying, $\Delta NO/O_3$ reached 74%. Therefore, the formation of the localized cooling zone was believed to suppress the thermal decomposition of ozone, and the NO oxidation performance of the system was either equal to or better than that of the previous laboratory experiments [18].

To compare the results obtained so far with the experimental conditions listed in **Table 2**, the dependence of the ratio of decrease in NO flow rates to the injected flow rate of O_3 ($\Delta NO/O_3$) on the average gas temperature at five measurement points at z = 2.85 m is analyzed, as shown in **Figure 9**. The results of our previous laboratory study [18] are also depicted herein. An equimolar ratio is employed in the oxidation reaction of NO and O_3 (moles of NO/moles of O_3 = 1). When the gas temperature is less than 50°C, $\Delta NO/O_3$ of more than 0.9 is achieved. However, $\Delta NO/O_3$ decreases with increasing gas temperatures up to ~300°C because of the decomposition of most of the injected O_3 into O_2, owing to the high temperature of the gas before the reaction with NO. The results

obtained at gas temperatures between 150 and 190°C (when the quantity of sprayed water is relatively large compared to that of the exhaust gas) are in good agreement with the trend exhibited by the results of the previous study; the results between 230 and 250°C (when the quantity of sprayed water is relatively small compared to that of the exhaust gas) show better $\Delta NO/O_3$ values than those of the previous study. This is because of the expansion of the cooling area to the temperature measurement zone (z = 2.85 m), owing to the relatively large quantity of water flowing via the three-fluid nozzle compared to that of the exhaust gas, which facilitates the proper evaluation of the NO oxidation field. However, when the quantity of sprayed water is relatively small compared to that of the exhaust gas, the cooling area does not extend into the temperature measurement area (z = 2.85 m). Therefore, the actual phenomenon involves NO oxidation with ozone in the duration when the spray from the three-fluid nozzle extends into the temperature measurement area (z = 2.85 m).

$\Delta NO/O_3$ is evaluated using the water spray flow rate for O_3, because it is difficult to modify the temperature measurement apparatus owing to the structure of the facility. **Figure 10** shows the dependence of $\Delta NO/O_3$ on the water spray flow rate for O_3. The solid line in the figure depicts an approximate linear least-squares fit in the injected ozone mass-flow-rate range of 9.3 to 11.2 kg/h. At a water spray flow rate of 0.15–0.17 m^3/h, $\Delta NO/O_3$ is higher when the injected ozone mass flow rate is in the lower range of 5.0 to 6.8 kg/h in the T2, T3 (Oct. 2019), and T2 (Nov. 2019) periods. This is because a higher injected mass flow rate of ozone leads to a larger localized cooling area that is required for NO oxidation; a low water spray flow rate for O_3 does not provide a sufficient localized cooling area for an injected ozone mass flow rate of 9.3 kg/h. In the injected ozone mass-flow-rate range of 9.3–11.2 kg/h, $\Delta NO/O_3$ increases as the water spray flow rate for O_3 increases. This is because the localized cooling area also increases with an increase in the water spray flow rate for O_3. Although $\Delta NO/O_3$ varies with the exhaust gas flow rate, $\Delta NO/O_3$ is greater than 0.6 when the water spray flow rate for O_3 is greater than 0.32 m^3/h, which is practically significant.

Sulfur oxide removal

Figure 11 shows the time-dependent SO_2 concentrations at the reactor inlet and outlet during the T1–T3 periods (July 2020). The average SO_2 concentrations at the reactor inlet and outlet in the T1, T2, and T3 periods are obtained as 404 ± 52, 436 ± 61, and 392 ± 45 ppm, and 346 ± 45, 305 ± 105, and 212 ± 52 ppm, respectively. SO_2 removal efficiencies of 14, 30, and 46% are achieved in the T1, T2, and T3 periods, respectively. These results reveal that the injection of ozone into the reactor increases desulfurization. Ozone is believed to transform SO_2 into SO_3, which activates the absorption reaction in the NaOH solution. The concentration of NaOH in T3 is higher than that in T2. Therefore, the desulfurization in T3 is higher than that in T2.

To compare these obtained results with the experimental conditions listed in **Table 2**, the variation of the decrease in SO_2 levels (ΔSO_2) with NaOH sprayed using the two-fluid spray nozzle is shown in **Figure 12**. The solid line in the figure represents the equivalent line corresponding to reaction (4). ΔSO_2 increases as the concentration of NaOH increases, and most of the obtained data are present above the equivalent line. The dust collected in the ESP was analyzed after the T4 test period (Oct. 2019) to confirm the reaction of SO_2 and NaOH. The results of this analysis reveal that the content of Na_2SO_4,

Na_2SO_3, Na_2CO_3, and $NaHSO_3$ are 92%, 1.7%, 2.8%, and 2.5% of the collected dust, respectively, implying that Na_2SO_4 and Na_2SO_3 are its major components. This indicates that most of the SO_2 reacts with NaOH to form SO_3^{2-} ions. Some of the SO_2 reacts with ozone to form SO_3, as mentioned previously; however, SO_3 reacts with NaOH to form Na_2SO_4. All the collected dust can be directly reused as glass material, and the reusable dust is approximately 0.1–1.0 mass % of the total raw material. Although the collection efficiency of the ESP depends on the desulfurization efficiency at the semi-dry reactor, a typical value of it was 98% with the concentrations of 1000 mg/m^{3}N at the ESP inlet and 20 mg/m^{3}N at the ESP outlet.

Nitrogen oxide removal

Oxidized NO_2 is reduced to N_2 by the SO_3^{2-} ion, as depicted in reaction (5), which is a byproduct of desulfurization in the localized cooling area. **Figure 13** shows the time-dependent NO_x concentrations at the reactor inlet and outlet during the T1–T3 periods (July 2020). The average NO_x concentrations at the reactor inlet and outlet in the T1, T2, and T3 periods are obtained as 230 ± 17, 200 ± 24, and 220 ± 22 ppm, and 232 ± 16, 134 ± 18, and 135 ± 17 ppm, respectively. The NO_x concentrations at the reactor inlet and outlet in the T1 period are observed to be similar. The NO_x component is mostly NO because the concentration of NO_x does not change, and, therefore, the denitration effect is not achieved. NO is oxidized to NO_2 in the T2 and T3 periods, resulting in a lower concentration of NO. The concentration of NO also decreases via the injection of O_3 into the localized cooling area and the NaOH solution spray. NO_x removal efficiencies of 0%, 33%, and 39% are therefore obtained in the T1, T2, and T3 periods, respectively. These higher NO_x removal efficiencies are better than those presented in a previous study [23] because of the increase in the quantity of injected ozone as well as the increase in residence time owing to the upward spray-injection-angle of the two-fluid nozzle.

It is considered that NO could be converted to higher oxides of nitrogen such as NO_3, N_2O_5, and N_2O by O_3. However, in this study, the concentrations of higher oxides of nitrogen productions are expected to be much less than that of NO_2 because the molar concentration of injected O_3 is lower than that of NO in the exhaust gas [24]. Furthermore, in our previous laboratory-scale simulated studies [18–21], the formation of N_2O was less than 3 ppm. It is considered that N_2O is scarcely induced in the O_3 injection denitration method.

To compare all the results obtained thus far with the experimental conditions listed in **Table 2**, the relationship between the decreased NO_x (ΔNO_x) and SO_2 (ΔSO_2), which contributes to the reduction of NO_2, is shown in **Figure 14**. The results of ΔNO_x corresponding to T1 (Nov. 2019, July 2020, and Aug. 2020) without ozone injection are absent in the figure because of negative ΔNO_x values. The solid line in the figure represents the equivalent line corresponding to reactions (4) and (5). As ΔSO_2 increases, ΔNO_x also increases, and most of the data are observed to be distributed around the equivalent line. This implies that the SO_2 removed by NaOH is converted to SO_3^{2-}, which in turn has almost completely removed the NO_2 oxidized by ozone. This is caused by the fact that the generated SO_3^{2-} instantaneously reacts with NO_x in the exhaust gas irrespective of oxygen concentration, which is considered an advantage of the simultaneous denitrification and desulfurization processes. However, considering that some of the SO_2 is converted to SO_3 by ozone as mentioned earlier, some of the NO_2 is

believed to react with water to yield nitrate or nitrite ions. From the figure, the results from the T2 (Oct. 2019), T3 (Oct. 2019), T2 (Aug. 2020), and T3 (Aug. 2020) periods are noted to be below the equivalent line. T2 (Aug. 2020) is almost the same as T3 (July 2020) in terms of the experimental parameters involved. However, ΔNO_x of the former is lower because ΔSO_2 is also reduced owing to the lower spray-flow-rate of the NaOH solution. Considering the experimental conditions of T2 (Oct. 2019), T3 (Oct. 2019), and T3 (Aug. 2020), where the water spray flow rate for O_3 and NaOH solution spray flow rate are in a ratio of 1:1, their respective ΔNO_x values are observed to be below the equivalent line. This is possibly because, as the water spray flow rate for O_3 increases, SO_2 becomes water soluble in the localized cooling region for O_3, resulting in an acidic solution that reacts with NO_2 to form HNO_3. The HNO_3 does not react well with SO_3^{2-}; however, it reacts with NaOH to neutralize it, which is presumed to result in a lower ΔNO_x. In any case, the SO_3^{2-} generated because of ΔSO_2 is confirmed to reduce NO_2 with high efficiency by increasing the NaOH solution spray flow rate compared to the water spray flow rate for O_3 and by maintaining the alkalinity of the reduction area.

Figure 14 also reveals that optimal ΔSO_2 and ΔNO_x concentrations of 180 and 85 ppm are achieved with experimental conditions corresponding to the T3 (July 2020) period, with removal efficiencies of 46% and 39%, respectively. The results of this study were obtained under a low amount of glass production and low exhaust gas flow rate. However, similarly high efficiencies for SO_2 and NO_x removal can be expected when the amount of glass production is increased and the exhaust gas flow rate is high. Additionally, it is possible to apply this technology to operate the glass melting furnace close to perfect combustion with high concentrations of SO_2 and NO_x emissions; the resulting energy savings can also be expected to reduce the amount of fuel input.

Energy efficiency

The results of this study thus far demonstrate that semi-dry PCHP can remove NO_x and SO_x with a high efficiency and energy savings. The energy efficiency of NO removal, that is, the ratio of the removed mass of NO to the ozonizer energy consumption are 74 and 84 g(NO_2)/kWh during the T2 and T3 periods in July 2020, respectively. It must be noted that the unit of g(NO_2) represents an equivalent mass of NO_x based on the molecular weight of NO_2. These values are higher than those obtained in our previous study (37 g(NO_2)/kWh with an injected O_3 mass flow rate of 1.2 kg/h) [23]. Compared to results from the previous study, the reason for the increase in energy efficiency via an increase in the quantity of ozone injected in this study involves the efficient oxidation of NO in the cooling region. To obtain the energy efficiency of NO_2 removal, the cost of NaOH (1.5 $/kg is assumed) is calculated using the power conversion cost (0.15 $/kWh) and the energy consumptions of NaOH in the T2 and T3 periods in July 2020 (107 and 216 kW, respectively). Therefore, the energy efficiencies of NO_2 removal during these periods are obtained as 55 and 34 g(NO_2)/kWh, respectively. Based on this, the energy efficiencies of NO_x removal by evaluating the electrical power using the cost of NaOH and the power consumption of ozonizers in the T2 and T3 periods in July 2020 are obtained as 29 and 23 g(NO_2)/kWh, respectively. The thermal input during the T2 and T3 periods in July 2020 is 9.3 MW, and the proportion of power consumption of both ozonizers and NaOH compared to the thermal input is only 2.1% and 3.3%, respectively. Na_2SO_4 produced during the simultaneous denitration and desulfurization can be reused, resulting in an

even lower energy consumption ratio that is acceptable by the glass manufacturing industry.

Table 3 lists the following results from this pilot-scale experiment: exhaust gas concentration at the reactor outlet; removal efficiencies of NO, NO_x, and SO_2; and energy efficiency of NO_x removal. The simultaneous treatment of NO_x and SO_x using the semi-dry-type PCHP with high efficiency was performed using a scale-up plasma ozonizer. The removal efficiencies of NO_x and SO_x can be increased by increasing the injected amounts of ozone and NaOH solution; it is possible to realize highly efficient and simultaneous desulfurization and denitrification with a significantly lower energy consumption than that in a glass melting furnace.

In the present tests, NO_x removal is lower than NO removal, depending on the operating condition. It means that the NO_2 produced by NO oxidation was not fully removed. The NO_2 should be completely removed by the optimization of operating conditions to realize an ideal denitration technology for glass-melting-furnace exhaust gas.

Conclusions

A pilot-scale experiment for NO_x and SO_x aftertreatment was conducted using a semi-dry PCHP in an exhaust gas treatment system for a glass melting furnace. High ozone injection conditions ($0.31 <$ moles of O_3/moles of $NO < 0.95$) with a scale-up plasma ozonizer setup confirmed that the simultaneous aftertreatment of NO_x and SO_x using the semi-dry-type PCHP was highly effective and promising for exhaust gas treatment from a glass manufacturing facility. The main results are summarized below:

(1) The temperatures at the reactor inlet and outlet were measured; the ~400°C exhaust gas at the inlet decreased to ~250°C at the outlet, but remained above the dew point. NO removal efficiencies of 42 and 45% were achieved in the NO oxidation experiment during the T2 and T3 test periods (July 2020). At an injected ozone mass flow rate between 9.3 and 11.2 kg/h, $\Delta NO/O_3$ increased as the localized cooling area expanded with an increase in the water spray flow rate for O_3.

(2) An SO_2 removal efficiency of 46% was achieved when the spray flow rate of the 3.0% NaOH solution was 0.7 m^3/h. Some of the SO_2 reacted with ozone to form SO_3; however, this was significantly dependent on the flow rate and concentration of the NaOH solution.

(3) NO_x removal efficiencies of 33% and 39% were obtained during the T2 and T3 test periods, respectively (July 2020). ΔNO_x increased as ΔSO_2 also increased, and most of these data were distributed around the equivalent line. This implied that the SO_2 removed by NaOH was converted to SO_3^{2-}, which in turn almost completely removed the NO_2 oxidized by ozone. This was caused by the fact that the generated SO_3^{2-} instantaneously reacted with NO_x in the exhaust gas irrespective of oxygen concentration, which is an advantage of the simultaneous denitrification and desulfurization processes.

(4) The byproduct analysis revealed that Na_2SO_4, Na_2SO_3, Na_2CO_3, and $NaHSO_3$ were obtained as 92%, 1.7%, 2.8%, and 2.5% of the total collected particulate matter, respectively. Na_2SO_4 and Na_2SO_3 are the major components of the collected dust and can be reused in glass manufacturing.

(5) Energy efficiencies of NO removal of 74 and 84 g(NO_2)/kWh were achieved during the T2 and T3 test periods, respectively (July 2020); these were an improvement over the results obtained previously with a lower ozone scale. The energy efficiencies of NO_x removal and total consumption of ozonizers and NaOH during the representative periods were 29 and 23 g(NO_2)/kWh and 2.1% and 3.3% of the thermal input to the glass melting furnace, respectively.

Acknowledgments

We would like to thank Dr. H. Fujishima, a researcher at Osaka Prefecture University, for his valuable advice on this work, and Mr. R. Tsuji and Mr. K. Yamakawa, members of Nihon Yamamura Glass Co., Ltd., for their support in carrying out the experiments.

Funding

This study is subsidized by a project fund (Strategic Innovation Program for Energy Conservation Technologies: JPNP12004) of the New Energy and Industrial Technology Development Organization (NEDO).

Conflict of interest

The author declares that they have no conflict of interest.

References

1. Li J, Chang H, Ma L, Hao J, Yang RT (2011) "Low-temperature selective catalytic reduction of NO_x with NH_3 over metal oxide and zeolite catalysts—a review". Cat Today 175:147–156. https://doi.org/10.1016/j.cattod.2011.03.034
2. Wang B, Pan Z, Du Z, Cheng H, Cheng F (2019) "Effect of impure components in flue gas desulfurization (FGD) gypsum on the generation of polymorph $CaCO_3$ during carbonation reaction". J Hazard Mater 369:236–243. https://doi.org/10.1016/j.jhazmat.2019.02.002
3. Majeed JG, Korda B, Békássy-Molnár E (1995) "Comparison of the efficiencies of sulfur dioxide absorption using calcium carbonate slurry and sodium hydroxide solution in an ALT reactor". Gas Sep Purif 9:111–120. https://doi.org/10.1016/0950-4214(95)93948-J
4. Yang B, Shen Y, Shen S, Zhu S (2013) "Regeneration of the deactivated TiO_2-ZrO_2-CeO_2/ATS catalyst for NH_3-SCR of NO_x in glass furnace". J Rare Earths 31:130–136. https://doi.org/10.1016/S1002-0721(12)60246-4
5. Noda S, Parwatha IG, Nada Y, Nishio S, Fukushige S (2007) Effect of flow field on NO_x emission properties of jet nonpremixed flames in cylindrical furnaces. J Environ Eng 2:730–739. https://doi.org/10.1299/jee.2.730
6. Zhou J, Zhou S, Zhu Y (2017) "Experiment and prediction studies of marine exhaust gas SO_2 and particle removal based on NaOH solution with a U-type scrubber". Ind Eng Chem Res 56:12376–12384. https://doi.org/10.1021/acs.iecr.7b02397
7. Min'ko NI, Binaliev IM (2013) "Role of sodium sulfate in glass technology". Glass Ceram 69:361–365. https://doi.org/10.1007/s10717-013-9479-8
8. Yamamoto T, Yang CL, Kravets Z, Beltran M (2000) "Plasma-assisted chemical process for NO_x control". IEEE Trans Ind Appl 36:923–927
9. Oda T, Kato T, Takahashi T, Shimizu K (1998) "Nitric oxide decomposition in air by using non-thermal plasma processing with additives and catalyst". IEEE Trans on Ind Applicat 34:268–272. https://doi.org/10.1109/28.663466
10. Okubo M, Kuroki T, Kitaura K, Yamamoto T (2006) "Diesel engine emission control using pulsed corona plasma-wet chemical hybrid process". J Environ Eng 1:29–38. https://doi.org/10.1299/jee.1.29
11. Cha MS, Song YH, Lee JO, Kim SJ (2007) "NO_x and soot reduction using dielectric barrier discharge and NH_3 selective catalytic reduction in diesel exhaust". Int J Plasma Environ Sci Technol 1:28–33. https://doi.org/10.34343/ijpest.2007.01.01.028
12. Yoshida K, Kuroki T, Okubo M (2009) "Diesel emission control system using combined process of nonthermal plasma and exhaust gas components' recirculation". Thin Solid Films 518:987–992. https://doi.org/10.1016/j.tsf.2009.07.171
13. Hayakawa Y, Inoue Y, Takeyama A, Kambara S (2016) "Reaction mechanism of de-NO_x by activated ammonia generated by dielectric barrier discharge". Int J Plasma Environ Sci Technol 10:20–23. https://doi.org/10.34343/ijpest.2016.10.01.020
14. Kuwahara T, Nakaguchi H, Kuroki T, Okubo M (2016) "Continuous reduction of cyclic adsorbed and desorbed NO_x in diesel emission using nonthermal plasma". J Hazard Mater 308:216–224. https://doi.org/10.1016/j.jhazmat.2016.01.034
15. Chang MB, Lee HM, Wu F, Lai CR (2004) "Simultaneous removal of nitrogen oxide/nitrogen dioxide/sulfur dioxide from gas streams by combined plasma

scrubbing technology". J Air Waste Manag Assoc 54:941–949. https://doi.org/10.1080/10473289.2004.10470965
16. Chang JS, Urashima K, Arquillq M, Ito T (1998) "Reduction of NO_x from combustion flue gases by corona discharge activated methane radical injections". Combust Sci Technol 133:31–47. https://doi.org/10.1080/00102209808952025
17. Zhou Q, Yao SC, Russell A, Boyle J (1992) "Flue gas NO_x reduction using ammonia radical injection". J Air Waste Manag Assoc 42:1193–1197. https://doi.org/10.1080/10473289.1992.10467067
18. Kuroki T, Yamamoto H, Fujishima H, Takada D, Yamato Y, Okubo M (2014) NO_x Removal for Flue Gas in Glass Furnace Using an Ozone Injection Chemical Hybrid Process -Laboratory Experiments with Semi-Dry Model System−. J Inst Electrostat Jpn 38:52-58 (in Japanese)
19. Yamamoto H, Kuroki T, Fujishima H, Takada D, Yamato Y, Okubo M (2014) "NOx removal from exhaust gas in a glass melting furnace using a plasma-chemical hybrid Process (From laboratory experiments to demonstration)". In: Proc. 9th international symposium non- thermal/thermal plasma pollution control technol sustain energy
20. Yamamoto Y, Yamamoto H, Takada D, Kuroki T, Fujishima H, Okubo M (2016) "Simultaneous removal of NO_x and SO_x from flue gas of a glass melting furnace using a combined ozone injection and semi-dry chemical process". Ozone Sci Eng 38:211–218. https://doi.org/10.1080/01919512.2015.1115335
21. Yamamoto H, Kuroki T, Fujishima H, Yamamoto Y, Yoshida K, Okubo M (2016) "A dry desulfurization and denitrification treatment for glass melting furnaces using plasma-chemical hybrid process technology". Trans Jpn Soc Mech Eng 82:16–00255 (in Japanese)
22. Yamamoto H, Kuroki T, Fujishima H, Yamamoto Y, Yoshida K, Okubo M (2017) "Pilot-scale exhaust gas treatment for a glass manufacturing system using a plasma combined semi-dry chemical process". IEEE Trans on Ind Applicat 53:1416–1423. https://doi.org/10.1109/TIA.2016.2616393
23. Yamamoto H, Kuroki T, Fujishima H, Okubo M (2019) "Pilot-scale NO_x and SO_x aftertreatment using a two-phase ozone and chemical injection in glass-melting-furnace exhaust gas". IEEE Trans Ind Appl 55:6295–6302. https://doi.org/10.1109/TIA.2019.2941423
24. Mok YS And Lee HJ (2006) "Removal of sulfur dioxide and nitrogen oxides by using ozone injection and absorption–reduction technique". Fuel Process Technol 87:591–597. https://doi.org/10.1016/j.fuproc.2005.10.007

Figure and Table captions

Fig. 1 Overview of the semi-dry aftertreatment system with the plasma chemical process, electrostatic precipitator, bag filter, and stack. The plasma ozonizers are located in a room on the left side of the apparatus.

Fig. 2 Schematic diagram of the semi-dry aftertreatment system with the plasma-chemical hybrid process for the glass melting furnace.

Fig. 3 Schematic of the nozzle arrangement for three-fluid (z = 1.85 m) and two-fluid sprays (z = 3.85 m).

Fig. 4 External view of the SAGT4M-C plasma ozonizer.

Fig. 5 (a) Interior structure of each reactor in the ozonizer and (b) side view of the SAGT6M-C ozonizer.

Fig. 6 Arrangement of temperature measurement points in the semi-dry reactor (one point at the inlet, five points each at z = 2.85 m and z = 4.35 m, three points at z = 5.85 m, and one point at the outlet).

Fig. 7 Time-dependent temperature of the exhaust gas at each measurement point at z = 0 m (reactor inlet), 2.85 m (reactor interior), 4.35 m (reactor interior), and reactor outlet in the T1–T3 test periods (July 2020).

Fig. 8 Time-dependent NO concentrations at the reactor inlet and outlet in the T1–T3 test periods (July 2020).

Fig. 9 Dependence of the ratio of decrease in NO to injected O_3 ($\Delta NO/O_3$) on the average gas temperature of the five measurement points at z = 2.85 m, featuring results from a previous study [18].

Fig. 10 Dependence of the ratio of decreased NO to injected O_3 ($\Delta NO/O_3$) on the injected water flow rate for O_3.

Fig. 11 Time-dependent SO_2 concentrations at the reactor inlet and outlet in the T1–T3 test periods (July 2020).

Fig. 12 Variation of the decrease in SO_2 with NaOH sprayed by the two-fluid spray nozzle.

Fig. 13 Time-dependent NO_x concentrations at the reactor inlet and outlet in the T1–T3 test periods (July 2020).

Fig. 14 Variation of the decrease in NO_x concentration with the decrease in SO_2 concentration.

Table 1 Specifications of ozonizers

Table 2 Experimental conditions and exhaust concentrations at the reactor inlet

Table 3 Exhaust concentrations at the reactor outlet, removal efficiency, and energy efficiency of NO_x removal.

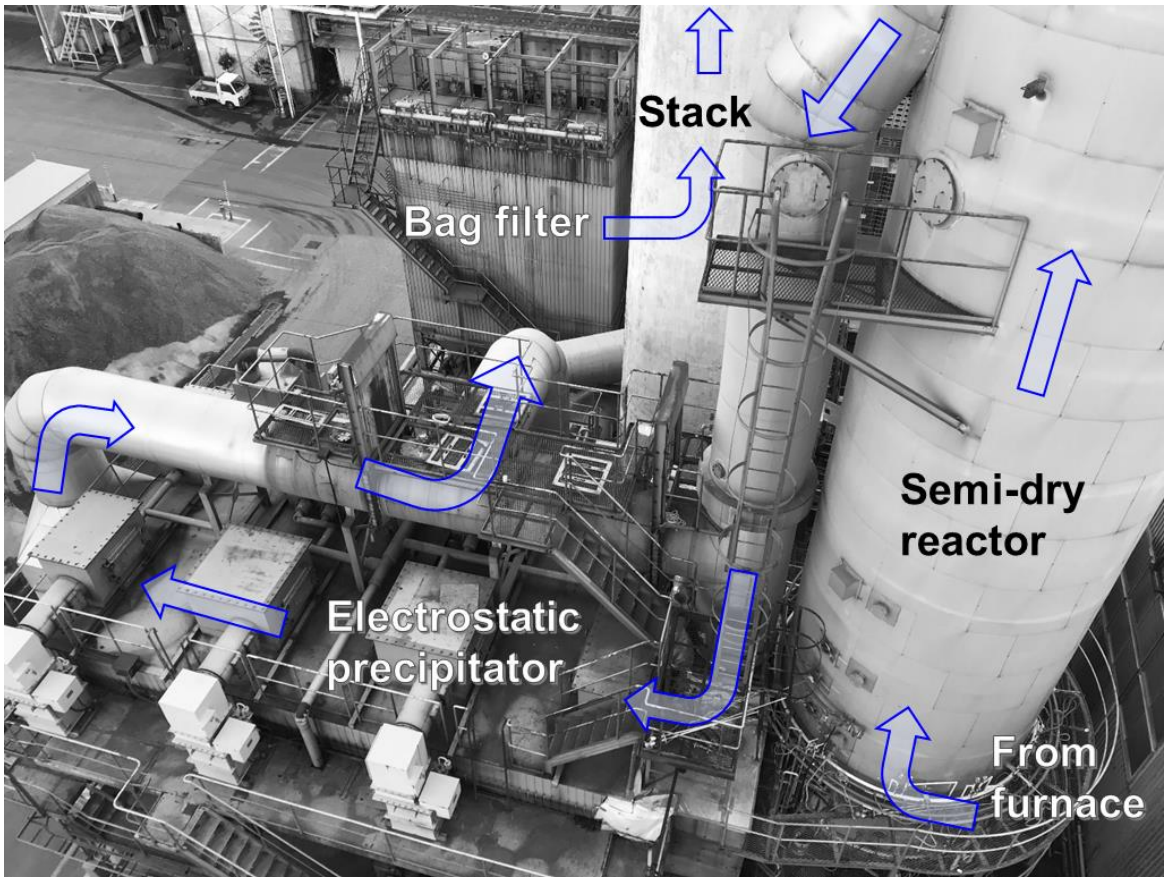
Stack
Bag filter
Semi-dry
reactor
Electrostatic
precipitator
From
furnace

Fig. 1

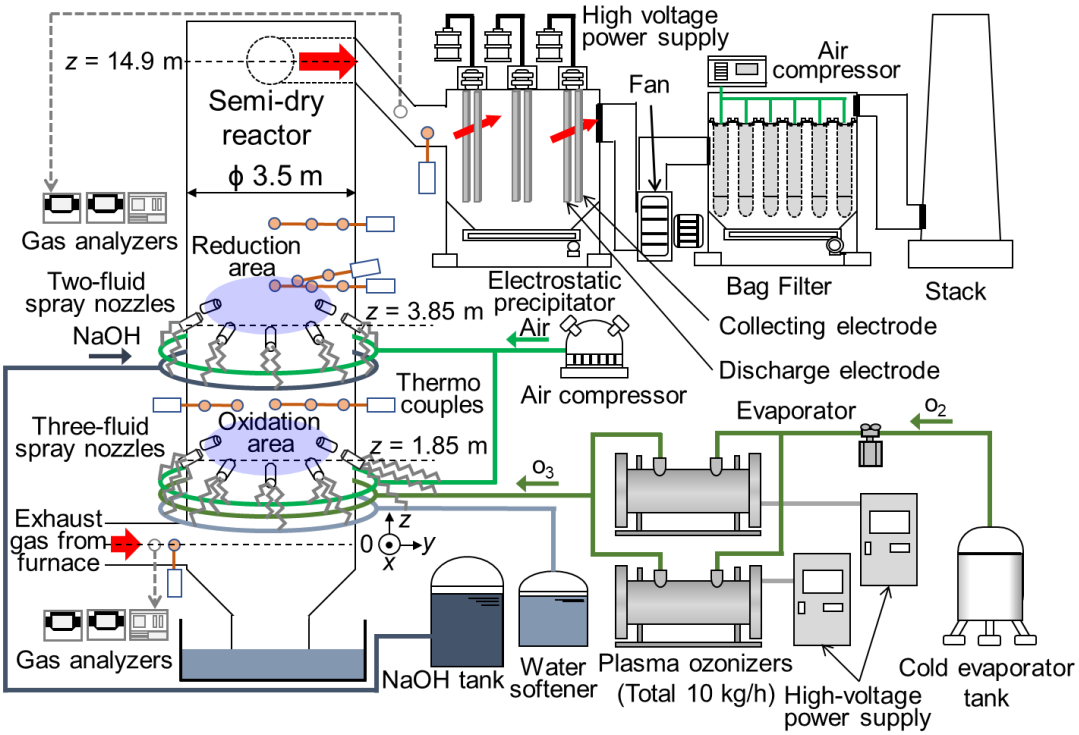
z = 14.9 m
Semi-dry
reactor
ϕ 3.5 m
Gas analyzers
Reduction
area
Two-fluid
spray nozzles
NaOH
z = 3.85 m
Thermo
couples
Three-fluid
spray nozzles
Oxidation
area
z = 1.85 m
Exhaust
gas from
furnace
Gas analyzers
High voltage
power supply
Fan
Air
compressor
Bag Filter
Stack
Electrostatic
precipitator
Air
Collecting electrode
Discharge electrode
Air compressor
Evaporator
O2
O3
z
0
y
x
NaOH tank
Water
softener
Plasma ozonizers
(Total 10 kg/h)
High-voltage
power supply
Cold evaporator
tank

Fig. 2

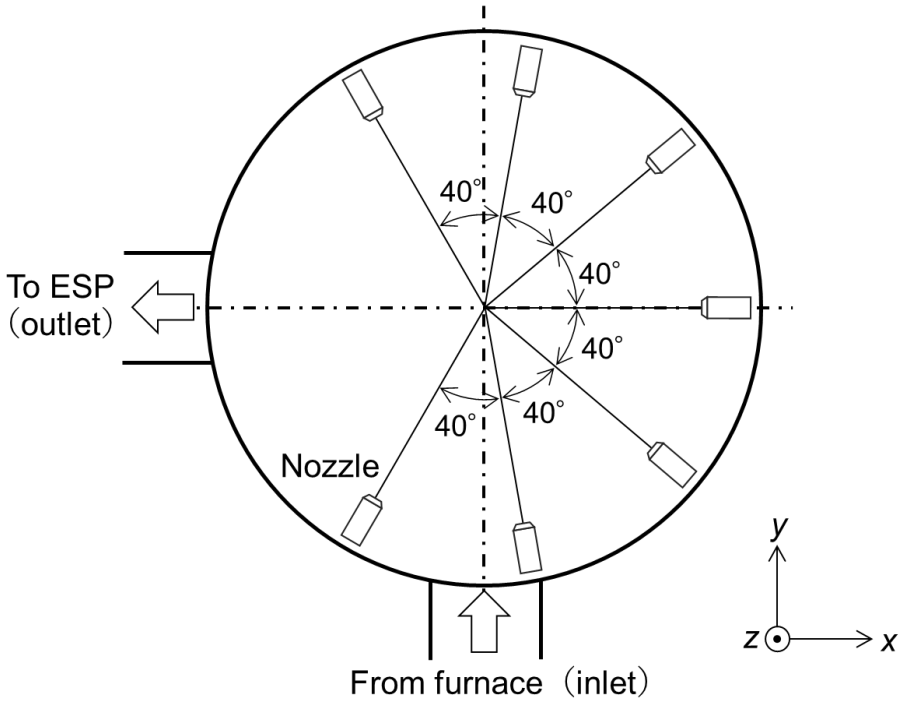

Fig. 3

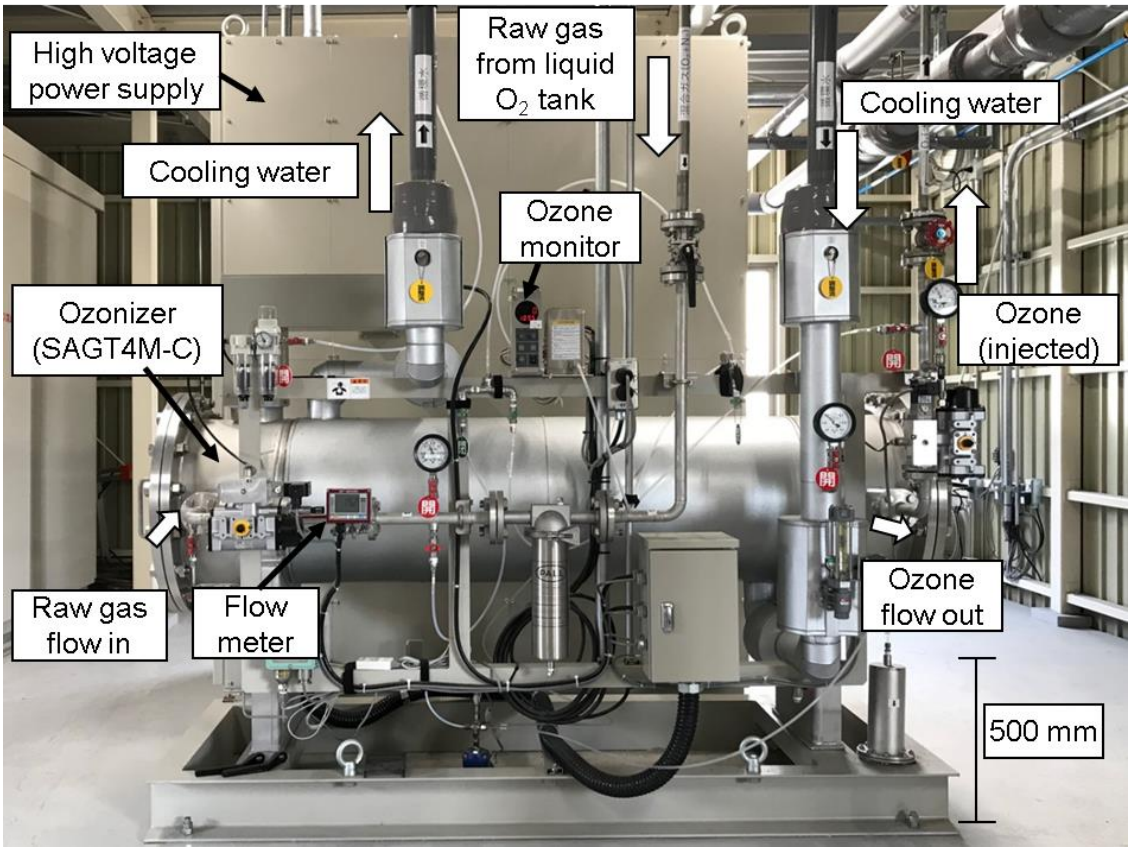
High voltage power supply
Raw gas from liquid O_2 tank
Cooling water
Cooling water
Ozone monitor
Ozonizer (SAGT4M-C)
Ozone (injected)
Raw gas flow in
Flow meter
Ozone flow out
500 mm

Fig. 4

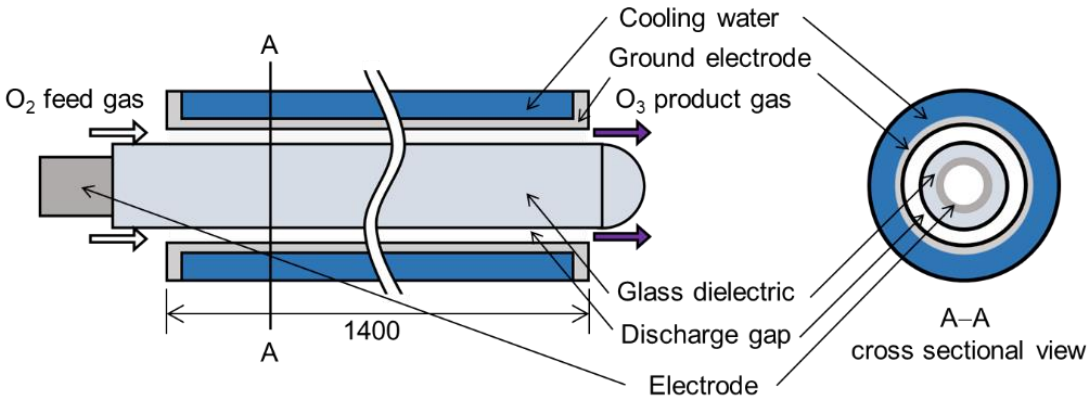

(a) Individual reactor

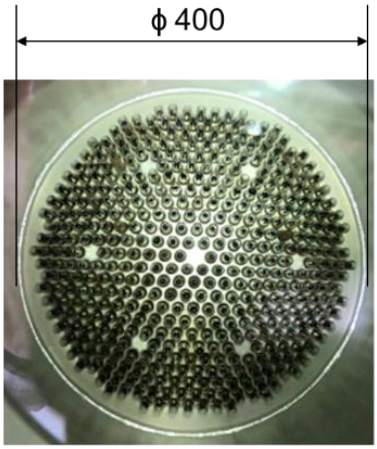

(b) Side view of the ozonizer

Fig. 5

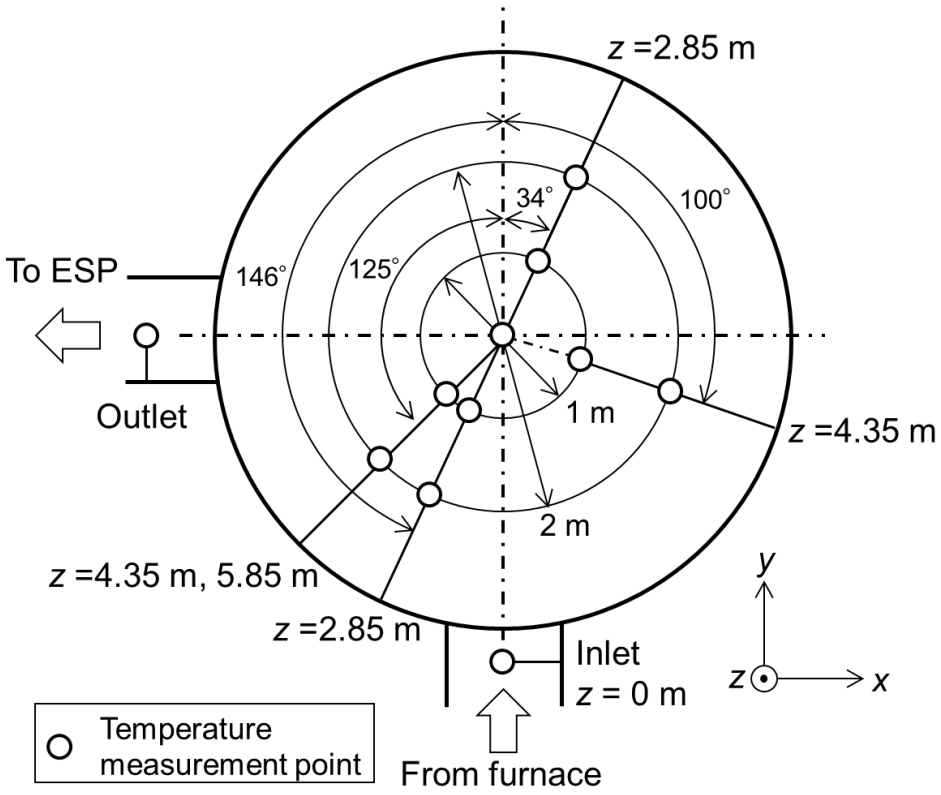
z =2.85 m
34°
100°
To ESP
146°
125°
Outlet
1 m
z =4.35 m
2 m
z =4.35 m, 5.85 m
z =2.85 m
Inlet
z = 0 m
y
z
x
Temperature measurement point
From furnace

Fig. 6

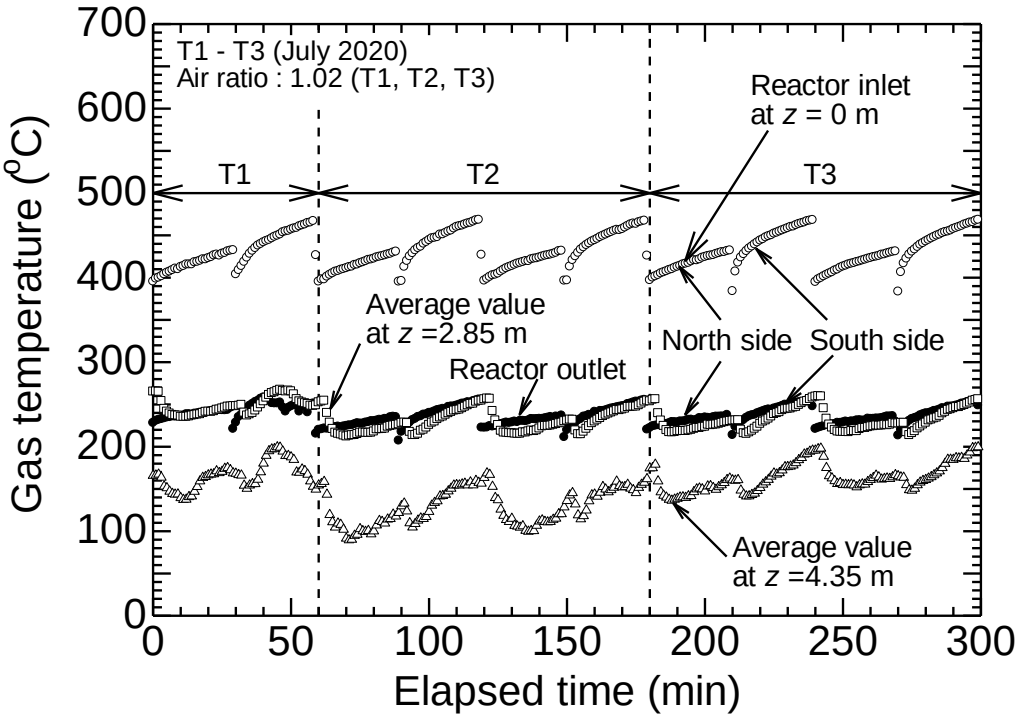
T1 - T3 (July 2020)
Air ratio : 1.02 (T1, T2, T3)
T1
T2
T3
Reactor inlet
at z = 0 m
Average value
at z =2.85 m
Reactor outlet
North side
South side
Average value
at z =4.35 m
Gas temperature (°C)
Elapsed time (min)
0
100
200
300
400
500
600
700
0
50
100
150
200
250
300

Fig. 7

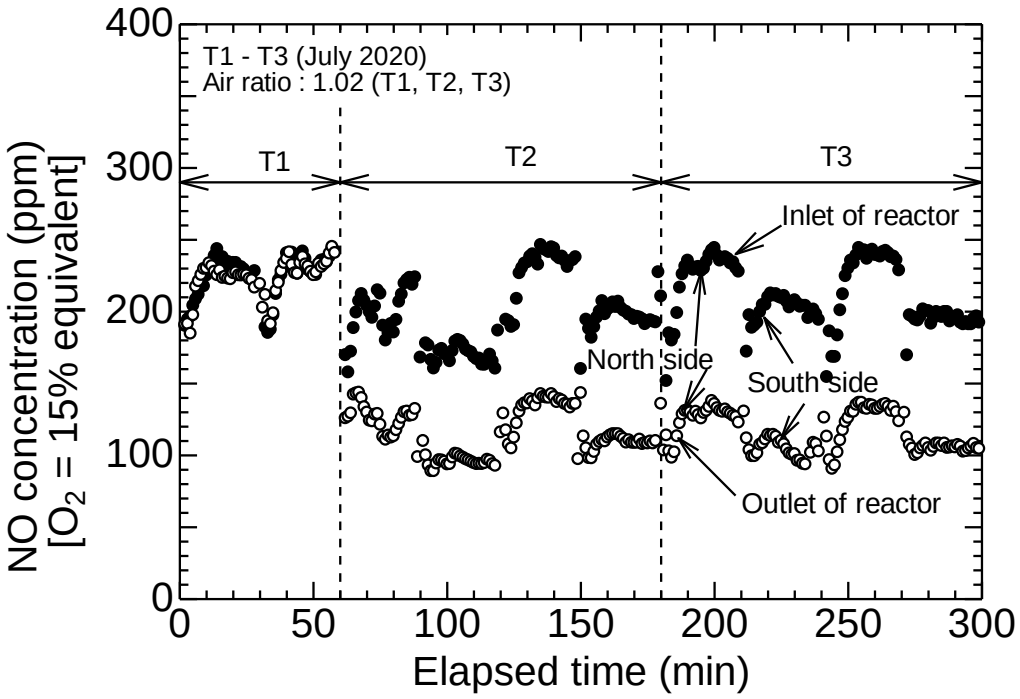
T1 - T3 (July 2020)
Air ratio : 1.02 (T1, T2, T3)
T1
T2
T3
Inlet of reactor
North side
South side
Outlet of reactor
NO concentration (ppm)
[O2 = 15% equivalent]
Elapsed time (min)
0
100
200
300
400
0
50
100
150
200
250
300

Fig. 8

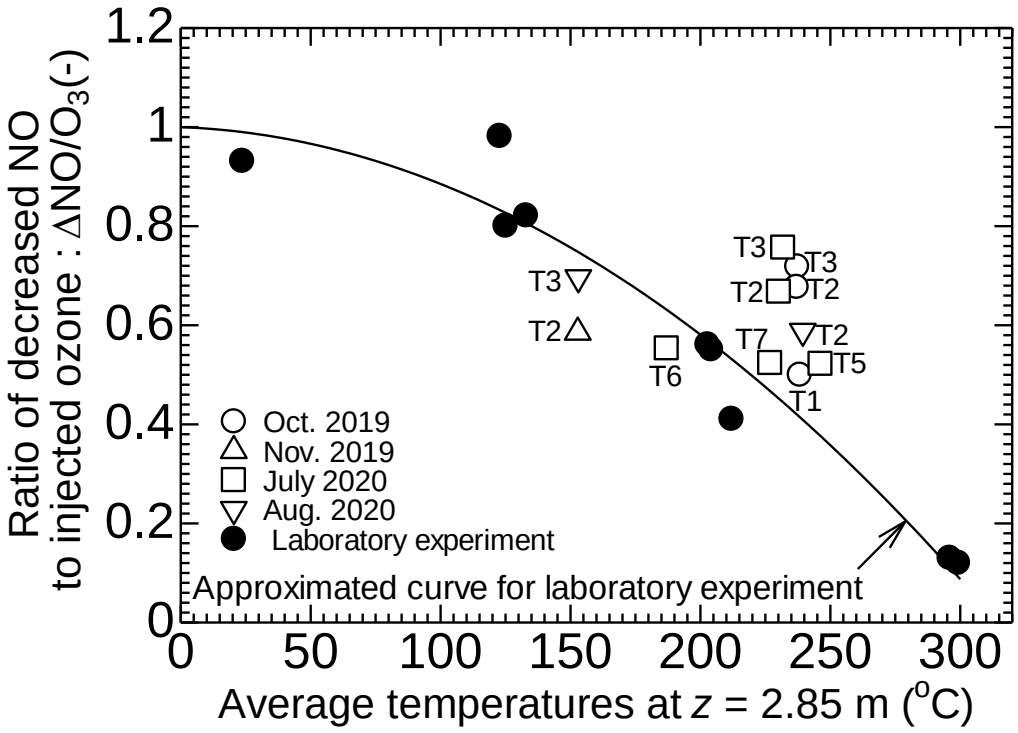
Ratio of decreased NO
to injected ozone : ΔNO/O3(-)
1.2
1
0.8
0.6
0.4
0.2
0
0
50
100
150
200
250
300
Average temperatures at z = 2.85 m (°C)
Oct. 2019
Nov. 2019
July 2020
Aug. 2020
Laboratory experiment
Approximated curve for laboratory experiment
T3
T2
T7
T6
T5
T1

Fig. 9

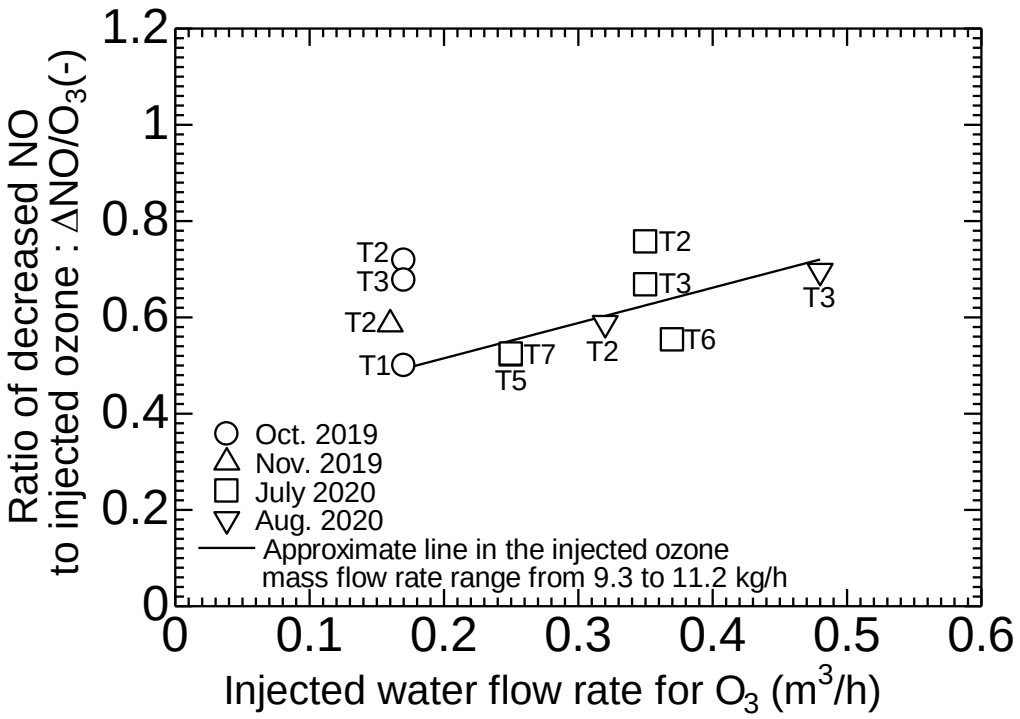
Ratio of decreased NO
to injected ozone : ΔNO/O3(-)
1.2
1
0.8
0.6
0.4
0.2
0
0
0.1
0.2
0.3
0.4
0.5
0.6
Injected water flow rate for O3 (m3/h)
T2
T3
T2
T1
T2
T3
T7
T5
T2
T6
T3
Oct. 2019
Nov. 2019
July 2020
Aug. 2020
Approximate line in the injected ozone
mass flow rate range from 9.3 to 11.2 kg/h

Fig. 10

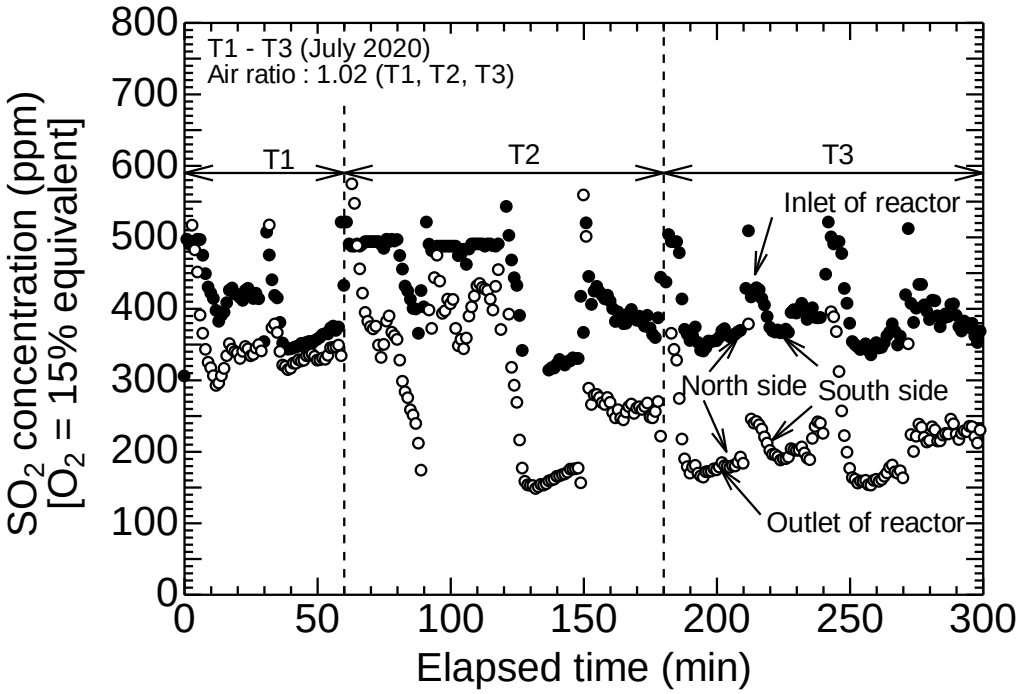
T1 - T3 (July 2020)
Air ratio : 1.02 (T1, T2, T3)
T1
T2
T3
Inlet of reactor
North side
South side
Outlet of reactor
SO2 concentration (ppm)
[O2 = 15% equivalent]
Elapsed time (min)
0
100
200
300
400
500
600
700
800
0
50
100
150
200
250
300

Fig. 11

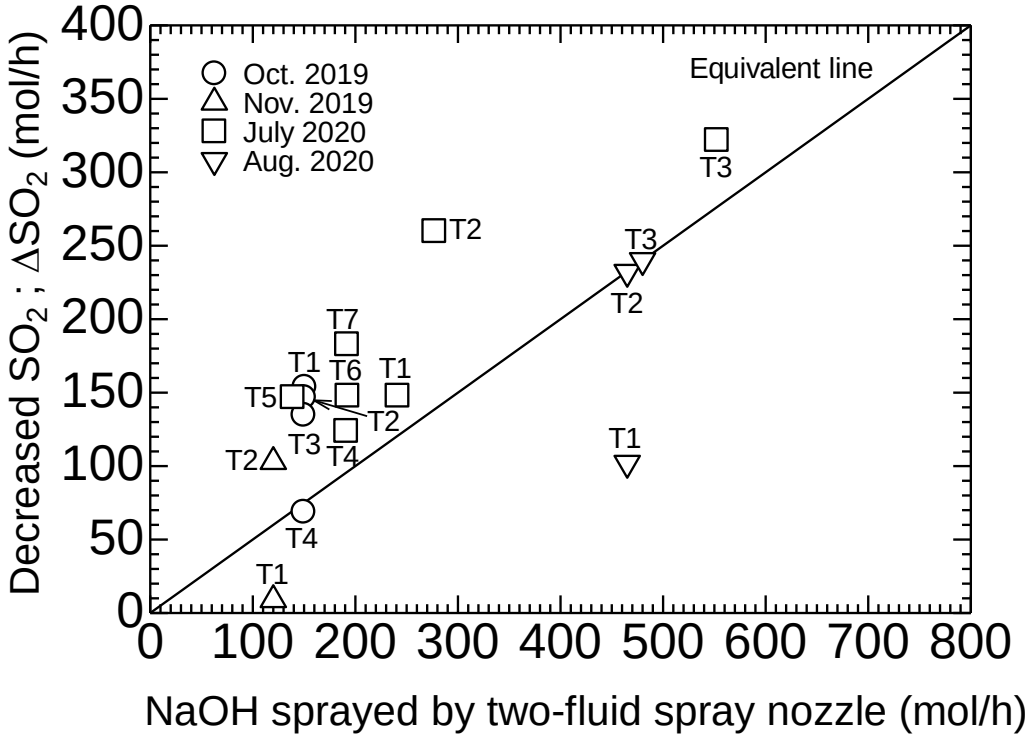
Decreased SO_2 ; ΔSO_2 (mol/h)
NaOH sprayed by two-fluid spray nozzle (mol/h)
Oct. 2019
Nov. 2019
July 2020
Aug. 2020
Equivalent line
0
50
100
150
200
250
300
350
400
0
100
200
300
400
500
600
700
800
T1
T2
T3
T4
T5
T6
T7

Fig. 12

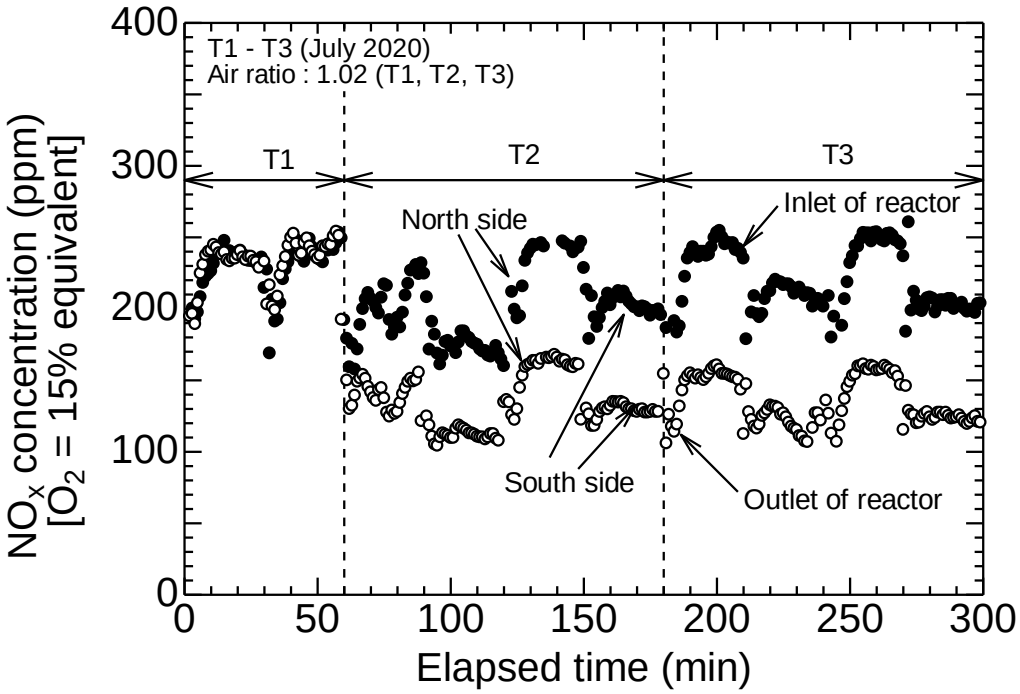
T1 - T3 (July 2020)
Air ratio : 1.02 (T1, T2, T3)
T1
T2
T3
North side
Inlet of reactor
South side
Outlet of reactor
NOx concentration (ppm)
[O2 = 15% equivalent]
Elapsed time (min)
0
100
200
300
400
0
50
100
150
200
250
300

Fig. 13

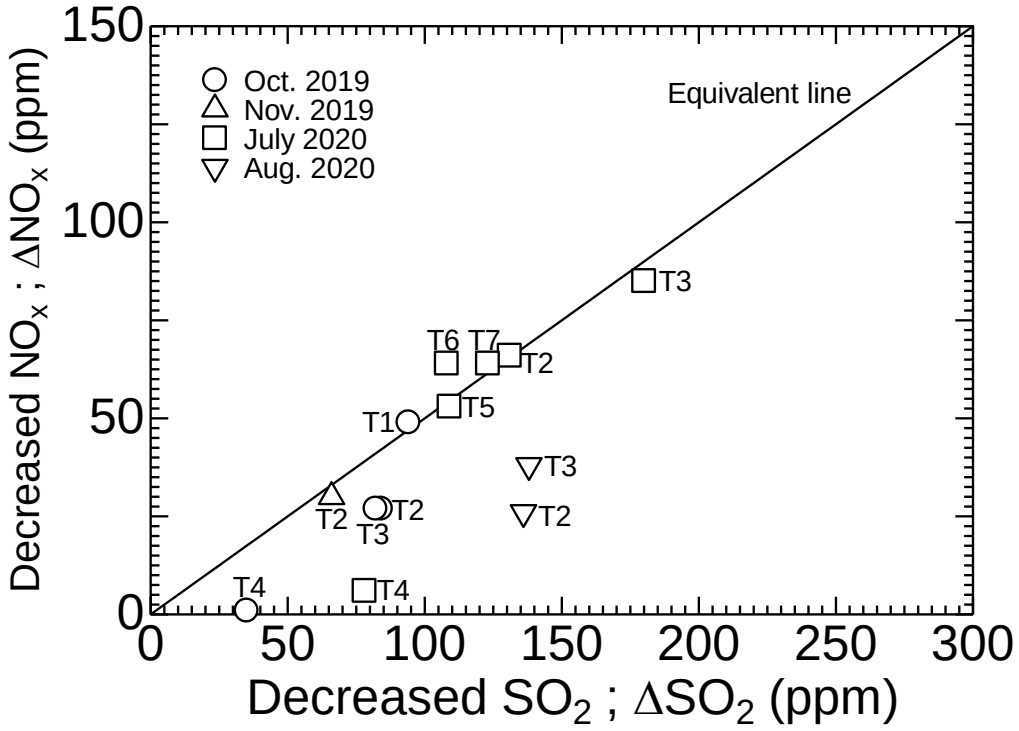
Oct. 2019
Nov. 2019
July 2020
Aug. 2020
Equivalent line
T3
T6
T7
T2
T5
T1
T3
T2
T2
T3
T2
T4
T4
Decreased NOx ; ΔNOx (ppm)
Decreased SO2 ; ΔSO2 (ppm)
0
50
100
150
200
250
300

Fig. 14

Table 1

Item	Specification	
Manufacturer	Sumitomo Precision Products Co., Ltd.	
Type	SAGT4M-C	SAGT6M-C
Plasma type	Dielectric barrier discharge with water-cooled electrodes	
Number of interior glass plasma reactors	334	432
Discharge voltage	5 kV	5 kV
Maximum ozone generation rate	4.0 kg/h	6.0 kg/h
Ozone concentration	150 g/Nm^3 = 7.0%	
Oxygen pressure at the inlet	0.13 MPa (gauge)	
Oxygen flow rate at the inlet	26.7 Nm^3/h	40.0 Nm^3/h
Oxygen pressure at the outlet	~0.12 MPa (gauge)	
Flow rate of cooling water	102 L/min	153 L/min
Temperature of cooling water at the inlet	15°C at the inlet (temperature difference is approximately 5°C)	
Width of ozone generation control	10–100% of the maximum generation	
Power consumption	28 kW	49 kW
Power source	AC400 V, three-phase, 50 Hz	

Table 2

Test group	Test periods	Exhaust gas volumetric flow rate (dry base)	Concentration of environmental load substances (average)			Gas temp. (inlet)	Injected O_3 mass flow rate	Water spray flow rate for O_3	NaOH solution spray flow rate	NaOH conc. for NaOH spray	Molar ratio of O_3/NO	Air ratio
		m^3N/h	NO ppm	NO_x ppm	SO_x ppm	°C	kg/h	m^3/h	m^3/h	%	-	-
(1) Oct. 2019	T1	13950	244	247	275	395	9.3	0.17	0.20	3.0	0.58	1.09
	T2	13650	245	248	272	395	5.0	0.17	0.20	3.0	0.31	
	T3	13600	243	245	276	393	4.9	0.17	0.20	3.0	0.31	
	T4	14050	234	234	269	390	0.0	0.17	0.20	3.0	0.00	
(2) Nov. 2019	T1	12900	194	196	342	414	0.0	0.15	0.16	3.0	0.00	0.98
	T2	12950	200	200	337	414	6.8	0.16	0.16	3.0	0.52	
(3) July 2020	T1	14700	225	230	404	442	0.0	0.30	0.64	1.5	0.00	1.02
	T2	14700	199	200	436	431	11.0	0.35	0.74	1.5	0.71	
	T3	14700	211	220	392	431	10.8	0.35	0.73	3.0	0.66	
	T4	11550	211	221	338	410	0.0	0.25	0.51	1.5	0.00	1.05
	T5	11550	197	207	337	410	10.9	0.25	0.51	1.5	0.93	
	T6	11950	193	197	326	409	11.0	0.37	0.37	1.5	0.93	
	T7	11950	190	196	320	409	11.0	0.25	0.51	1.5	0.95	
(4) Aug. 2020	T1	14400	226	228	426	416	0.0	0.32	0.62	3.0	0.00	1.03
	T2	14400	216	211	409	413	11.2	0.32	0.62	3.0	0.70	
	T3	13900	223	227	399	412	11.0	0.48	0.48	4.0	0.66	

Table 3

Test group	Test periods	Exhaust gas volumetric flow rate (dry base)	Concentration of environmental load substances (average)			Gas temp. (outlet)	Removal efficiency			Energy efficiency of NO_x removal
			NO	NO_x	SO_x		NO	NO_x	SO_x	
		m^3N/h	ppm	ppm	ppm	°C	%	%	%	$g(NO_2)$ /kWh
(1) Oct. 2019	T1	14600	193	198	181	262	21	20	34	27
	T2	14350	218	221	188	264	11	11	31	33
	T3	14250	213	218	194	264	12	11	30	29
	T4	14450	230	233	234	264	2	0	13	
(2) Nov. 2019	T1	14800	213	207	333	278	-10	-6	4	
	T2	14850	142	169	277	279	29	15	17	21
(3) July 2020	T1	16000	223	232	346	247	1	-1	14	
	T2	16000	116	134	305	235	42	33	30	29
	T3	16000	116	135	212	236	45	39	46	23
	T4	13450	208	215	260	237	1	3	23	
	T5	13450	106	154	228	239	46	25	32	20
	T6	14000	97	133	218	240	50	32	33	27
	T7	14000	107	132	197	235	44	33	38	27
(4) Aug. 2020	T1	16000	240	240	353	248	-6	-5	17	
	T2	16000	134	185	273	242	38	12	33	10
	T3	15100	128	189	261	236	43	16	35	12